Parameter Estimation of Three-Phase Transformer Models for Low-Frequency Transient Studies from Terminal Measurements

Qiong Wu, *Student Member, IEEE,* Saeed Jazebi, *Member, IEEE,* and Francisco de Leon, *Fellow, IEEE*

Department of Electrical and Computer Engineering, New York University, New York 11201, USA

This paper introduces a three-phase reversible transformer model for the study of low-frequency transients. The model topology is obtained from the direct application of the principle of duality by drawing basic circuit elements on top of the transformer frame. The model parameters are obtained from terminal and physical size measurements as well as the characteristics of the iron core. The implementation of the model is based on standard drag-and-drop circuit elements available in electric circuit simulation programs. The model is validated with inrush current and normal open circuit laboratory measurements. The main advantage of this model is that the parameters remain the same for the simulation of different operating conditions from all terminals. This is true for transients involving deep saturation, normal loading operation, or open circuit.

Index Terms— **Electromagnetic transients, low-frequency transients, power transformers, principle of duality, transformer modeling.**

I. INTRODUCTION

FERROMAGNETIC material is widely used in power transformer cores. Due to the magnetic nonlinearity of the iron core, low-frequency transients, such as inrush current, ferroresonance and geomagnetic induced current (GIC) usually happen when the transformer is driven to high saturation. In saturated conditions, the magnetic behavior of the iron core is substantially different when compared to normal operating conditions. Most of commercially available electromagnetic transient simulation programs offer three-phase transformer models that are built from three single-phase transformer unit models. Therefore, the geometrical information and physical properties of the transformers are not considered properly and thus vital magnetic phenomena are not represented correctly. Additionally, changes in model parameters are necessary for most of the available models when dealing with different operating conditions.

Transformer models for transients are usually specialized for a band of frequency [1]-[3]. For example, models for low frequency transients are developed for phenomena between dc and 3 kHz. The response of a three-phase transformer to a low-frequency transient differs from phase to phase and from winding to winding (primary, secondary, and tertiary). This is so because the most significant parameters in deep saturation region are terminal resistance and saturation inductance that vary for primary, secondary, and tertiary winding of different phases. Hence, a transformer model that is accurate to estimate inrush currents, ferroresonance, and GIC seen from all terminals, without modification of parameters, introduces technical/mathematical modeling challenges.

There is a gamut of models for three-phase transformers [4]-[20]. Some of them can be used for a wide range of frequencies, including low-frequency transients [4]-[9]; some are solely applicable for low-frequency transients [10]-[20]. Among these, some are introduced for the calculation of inrush currents [13]-[18]; some are applicable for the computation of ferroresonant over-voltages [8], [19], [20]; and a few of them are specifically developed for the calculation of GIC [8]. However, they all need parameter adjustments to represent the terminal behavior of different windings of different phases.

A dual model for single-phase two-winding transformer was proposed in [21] and [22]. The model adequately replicates the low-frequency behavior of the transformer especially in high saturation seen from all terminals. This is possible because the model represents saturation inductance and winding resistance of the transformer from primary and secondary windings, simultaneously. As a result, this model is called “reversible,” since it can predict transients from both terminals without any parameter adjustments [22]. The model was further developed for single-phase multi-winding transformers in [23].

In this paper, the reversible model of [21] and [22] is extended to three-phase transformers. First, a topological three-phase transformer model is derived based on the direct application of the principle of duality over the transformer structure. The tank is included in the model considering the magnetic flux paths in high saturation and under unbalanced operation. Parameter identification methods in deep saturation and in normal operation conditions are introduced. For illustration, a three-leg (core-type) transformer is modeled. The parameters are calculated based on data collected from terminal measurements, external dimensions, and datasheets of the iron core material. The model is then implemented in the Electromagnetic Transients Program (EMTP) [24], and validated versus normal open circuit measurements and inrush currents. Due to space limitations, only a three-leg stacked-type transformer is illustrated. However, a similar technique can be applied to other core types. Experimental validation of the method applied to a five-leg wound core and Evans core transformers will be presented in a forthcoming paper.

II. MODELING PRINCIPLES

A dual transformer model consists of leakage inductances, magnetizing inductances, ideal transformers, and resistive elements. Unlike single-phase transformers, three-phase transformers can have different terminal connections (Δ, Y, Zigzag)

Corresponding author: Q. Wu (e-mail: qw388@nyu.edu).

Color versions of one or more of the figures in this paper are available online at http://ieeexplore.ieee.org.

Digital Object Identifier (inserted by IEEE).

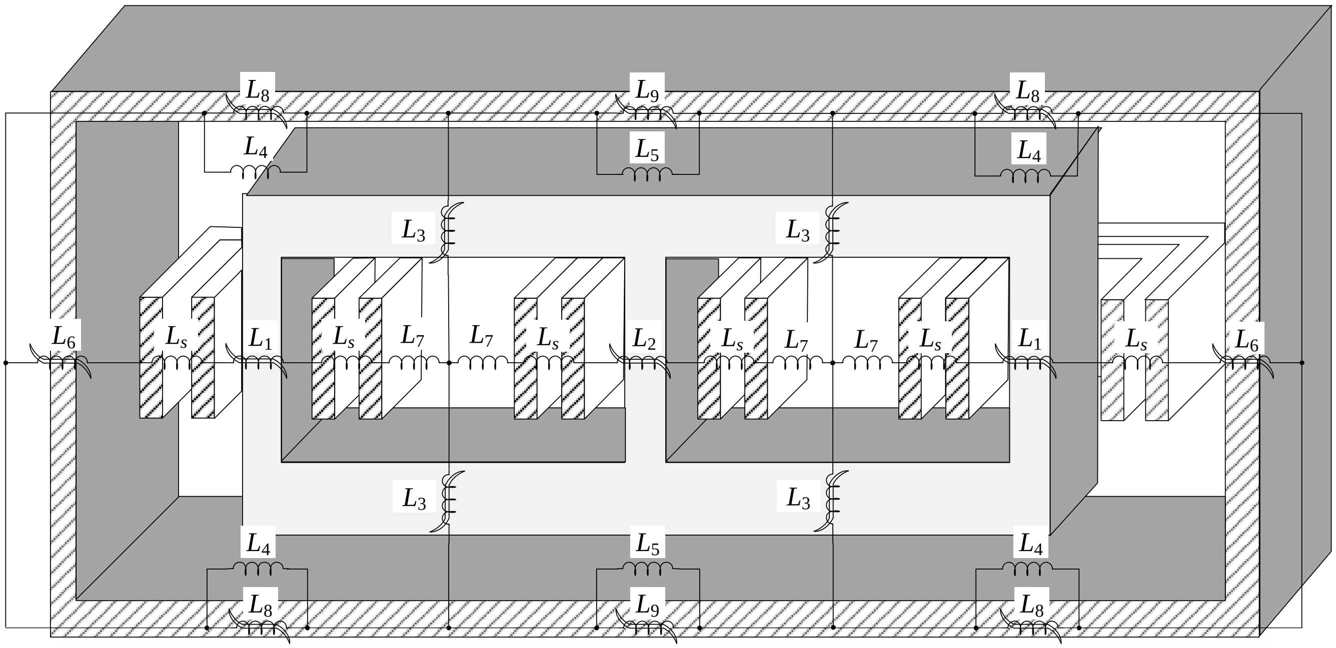

Fig. 1. Topology of the dual reversible model for the core-type three-phase transformer with two windings and the tank.

which add complications to the modeling. In practice, the Δ-Y connection is the most popular configuration. Hence, it is the one selected for the case study in this paper. Note however, that other connections can be implemented following the same principles.

A. Topological Model

Fig. 1 illustrates the geometry of a three-phase, core-type (three-leg), two-winding transformer. In each phase, the inner and the outer windings are shown, representing the secondary and the primary, respectively. The electrical equivalent circuit is derived from the direct application of the principle of duality superimposed on the transformer frame. Each element is placed on its physical counterpart. To avoid confusions, the terminal connections and ideal transformers are not shown in this figure; however, they can be easily connected at the physical locations of the windings. Ideal transformers are necessary for the following reasons [25]: they isolate the magnetic equivalent circuit (inductors) from the electrical circuit (resistors and capacitors); they are significant when making external connection (Y/Δ), avoiding unfavorable short circuits in the terminals. Both the core and the tank are modeled with hysteretic inductors [26], [27].

There are two types of inductors in the equivalent circuit of Fig. 1. The first category consists of hysteretic inductors L_1, L_2, L_3, L_6, L_8 and L_9. These inductors represent the nonlinear magnetizing characteristics of the core as well as the tank. The second category includes linear inductors L_s, L_4, L_5 and L_7. These linear inductors are mainly used to represent magnetic flux distribution in air. Leakage inductances L_s need to be modeled by linear components. This is so because, in open circuit conditions with nominal voltage, there is no leakage flux (inductance) [22], [23]. Leakage inductance is defined to represent the magnetic energy confined between two windings that mutually interact in order to transfer energy from one to another. Since the secondary winding is open in this condition, there is no leakage field, and as a result the leakage inductance loses its meaning. Therefore, the leakage inductance only appears for a transformer under load or short circuit. This inductance does not change significantly in these two conditions. Thus, it could be modeled as a linear inductor.

To compute all aforementioned types of inductors three conditions, i.e. short circuit, normal open circuit, and deep saturation, are considered.

In short circuit or normal operation conditions, the magnetizing branches (hysteretic inductors) are in parallel with the terminals and operate around the knee point of the saturation curve. Therefore, their impedance is high and they are commonly neglected when deriving the equivalent impedance from the terminals.

As discussed, leakage inductance does not exist in open circuit conditions. This is while the components L_s still exist in the equivalent circuit of Fig. 1. However, these parameters can be neglected, because their value is very small when compared to the magnetizing branches in normal open circuit condition. Therefore, there is no need to remove them from the equivalent circuit when modeling this condition.

In high saturation conditions, however, all the magnetizing branches (hysteretic inductors) operate in the region above the knee point. In this region, the slope of the magnetizing inductors, the so-called the saturation inductance, is comparable to the leakage inductance [22]. Hence, inductances L_s can no longer be neglected when calculating equivalent inductances from terminals.

In the saturation region, it is very important that the equivalent inductance seen from all terminals matches the saturation inductance of the corresponding windings. Thus, special care is needed when computing the saturation inductance of the hysteretic branches.

This article has been accepted for publication in a future issue of this journal, but has not been fully edited. Content may change prior to final publication. Citation information: DOI 10.1109/TMAG.2016.2563389, IEEE Transactions on Magnetics

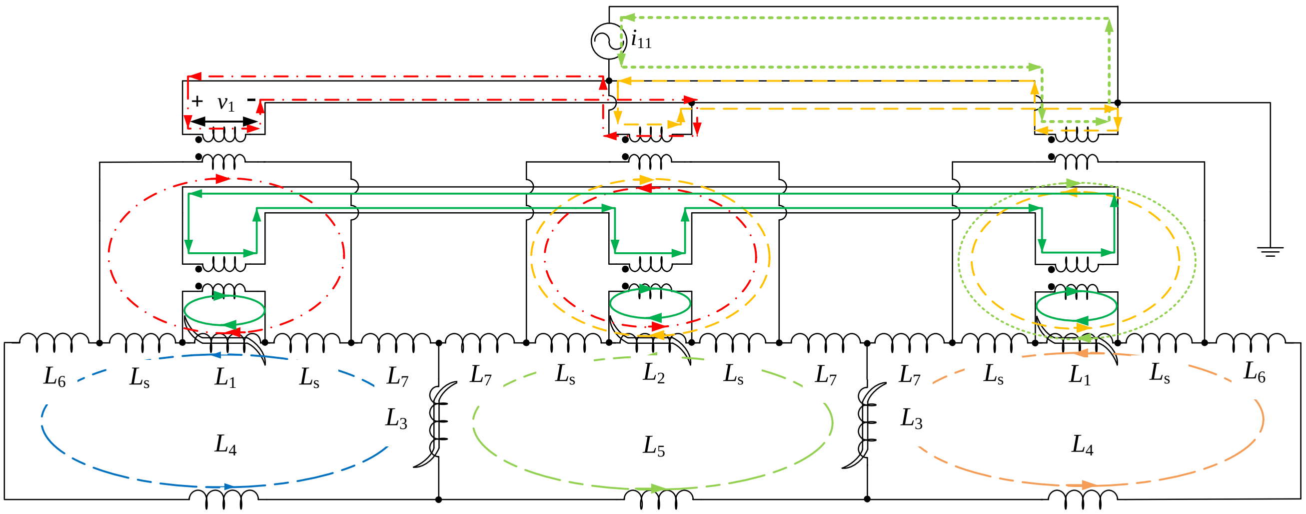

Fig. 2. Simplified dual reversible model for three-phase two-winding transformer in Test 1 considering the ideal transformers. The proper selection of the mesh currents is demonstrated. The ideal transformers change the direction of the mesh as shown in this figure. This behavior must be considered when writing the circuit equations. Note that, the terminal resistances are not added since the objective is to derive the equivalent inductance of the model seen from the terminals. They can be simply added in series to the source side of all ideal transformers.

B. High Saturation Condition

The most important component for transients involving deep saturation, such as inrush currents is the saturation inductance of the transformer seen from all terminals. Therefore, one needs to be able to compute it with adequate accuracy. In deep saturation, transformer iron core is operating in the linear region, high above the saturation point. The saturation of grain oriented steel is dependent on silicon content and grain orientation [33]. Established modelling methods use polynomial or exponential extrapolations after the final measured point of the magnetization curve; see [34], [35]. However, when all limbs and yokes are completely saturated, the incremental inductance is equal to having the windings in air yielding the so-called air-core inductance. Therefore, the hysteretic inductors in this region can be simplified as linear inductors having an air core with permeability equal to μ_0.

To identify the model parameters in this region, the inductance network of Fig. 1 is solved considering that all inductors are linear. Then mesh equations are written to obtain the system matrix. Considering the fact that the mathematical solution needs to be equivalent to the set of terminal measurements in the deep saturation region, a system of equations is written.

Necessary simplifications are made on the inductance network of Fig. 1. For example, inductors L_4, L_5 and L_8, L_9 are in parallel, respectively. In normal open circuit (unsaturated) condition, L_4 and L_5 are relatively small, because of the high reluctance of the gap between the transformer and tank. Hence, in normal open circuit, L_8 and L_9 that are represented by hysteresis curves, could be neglected (almost shorted by L_4 and L_5), when excited by three-phase balanced source. This phenomenon is physically sound, because balanced three-phase flux remains in the core and could not penetrate the top part of the tank due to the high reluctance of air (oil). In high saturation conditions (balanced or unbalanced), L_8, and L_9 behave as linear inductors in saturated regions of the tank. Consequently, the linear part represents the equivalent slope of L_8 and L_9 in parallel with L_4 and L_5. Therefore, for simplicity, L_8 and L_9 can be merged into L_4 and L_5, respectively. Note that, after final calculation of these equivalent inductances, results should be decomposed again into separate components L_4, L_5, L_8, and L_9 according to magnetic properties and dimensions of tank, gap spaces, and the solution of optimization method introduced in the next section. The reduced circuit is depicted in Fig. 2. After simplifications, seven unknowns still remain (L_1, L_2, L_3, L_4, L_5, L_6 and L_7), that need to be calculated. Therefore, to have a unique solution, seven equations need to be derived from terminal measurements. Seven special tests are introduced in the following subsections. The results of these measurements are used along with the equations to obtain the model parameters. Note that, the leakage inductor L_s can be measured directly from short circuit tests, as shown in the next section.

1) Measurements

Fig. 3 portrays seven tests proposed in this paper to calculate the parameters. To ensure the saturation of the transformer during the tests, a hybrid source that consists of a dc source in series with an ac source can be used [28]. Note that, however, the voltages (v_i) and currents (i_{i1}) in Fig. 3 are fundamental components of the measured signals.

The different connections (Y/Δ) change the solution of the electric circuit seen from terminals. The high voltage and low voltage sides are connected in Y and Δ, respectively. In the proposed tests, the secondary voltage (in open circuit) is always recorded. This is to avoid the measurement of voltage drop on the winding resistance that guarantees consistent recording of the internal voltage (the voltage related to the linkage flux). Note that, Test 1 is an exception with this respect, where the voltage is measured from primary. Test 1 represents the zero-sequence test in presence of Δ. This connection does not provide any path for the zero-sequence current. Hence, the measured voltage is always zero from the open circuit secondary.

This article has been accepted for publication in a future issue of this journal, but has not been fully edited. Content may change prior to final publication. Citation information: DOI 10.1109/TMAG.2016.2563389, IEEE Transactions on Magnetics

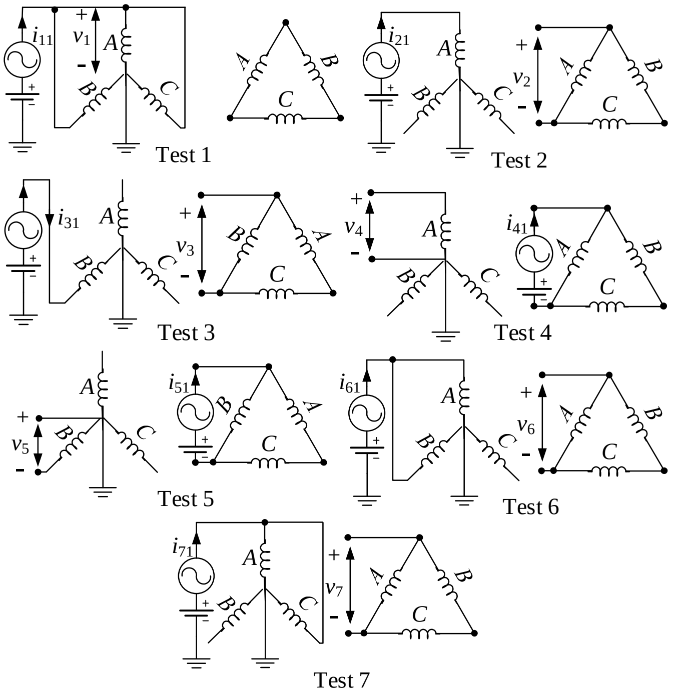

Fig. 3. Seven tests used to derive the saturation characteristics of the hysteretic inductors.

The measured inductances obtained from the terminals through the seven tests (Test 1, Test 2, …, Test 7) are denoted as L_{sat1}, L_{sat2}, ... L_{sat7}. For Tests 2 to 7, the values of the saturation inductance could be computed with the following expression [28]:

$$L_{sat,i}=\frac{v_i}{j\omega k\, i_{i1}},\quad i=2,...,7 \tag{1}$$

where k is the turns ratio, ω is the angular frequency, and j is the imaginary unit. For Test 1, the voltage is measured from primary. Hence, the voltage drop on the primary winding resistance is included in the voltage measurements. In this test, three primary windings (with R_{pw}) are in parallel. Therefore, the saturation inductance can be expressed as:

$$L_{sat1}=\frac{1}{\omega f\, k}\sqrt{\left(\frac{v_1}{i_{11}}\right)^2-\left(\frac{R_{pw}}{3}\right)^2} \tag{2}$$

2) Analytical Equations

To explain the procedure to obtain the equations, Test 1 is selected as an example. The following two major steps are used:

Step 1: Seven meshes are selected in the magnetic circuit of Fig. 2. The meshes of other 6 tests can be deduced from the meshes in Fig. 2. The fundamental format of the mesh equations for the i^{th} test (i = 1 in this example), is:

$$j\omega K_{i,n\times n} I_{i,n\times 1}=V_{i,n\times 1} \tag{3}$$

$$I_i=[i_{i1},i_{i2},i_{i3},...i_{in}]^{\mathrm{T}},V_i=[v_i,0,0,...0]^{\mathrm{T}} \tag{4}$$

where n=7 is the number of meshes, I_i, and V_i are current and voltage vectors, where their elements are the currents of the meshes and the voltage sources, respectively (see i_{i1} and v_i in Fig. 3, and i_{11} and v_1 in Fig. 2). As discussed before, v_i is measured on the secondary side (see Fig. 2), except for Test 1. For Test 1, the v_1 represents primary voltage minus voltage drop on primary windings. All equations in this paper are referred to primary.

Step 2: Matrix K is reduced to an algebraic equation. Note that, this matrix consists of four components as follow:

$$K_{i,n\times n}=\begin{bmatrix} A_{i,1\times 1} & B_{i,1\times(n-1)} \\ B_{i,1\times(n-1)}{}^T & D_{i,(n-1)\times(n-1)} \end{bmatrix} \tag{5}$$

Since the voltage vector of (4) has only one nonzero element, Kron reduction can be applied to decrease the dimensions of the inductance matrix [23]:

$$L_{eq,i}=A_i-B_iD_i^{-1}B_i^T=f_i(L_1,L_2,L_3....,L_7) \tag{6}$$

where $L_{eq,i}$ stands for the equivalent inductance seen from terminal i, for i=1,2,…7, that is a function of L_1 to L_7. Equation (7) (shown at the bottom of the page) is the equivalent inductance expression for Test 1. The other 6 equations are not presented because of the lack of space. However, they could be found in reference [29].

Note that, for the set of the seven tests of Fig. 3, the following equation should be satisfied:

$$j\omega L_{eq,i}\, i_{i1}=v_i \tag{8}$$

3) Solution of the Saturation Inductances

The resultant algebraic equations obtained in previous steps for L_{eq1} to L_{eq7} are made equivalent to the measured inductances L_{sat1} to L_{sat7}. Therefore, the following objective function is to be minimized to obtain the unknowns:

$$f_{object}=\min\left[(L_{eq1}-L_{sat1})^2+\cdots+(L_{eq7}-L_{sat7})^2\right] \tag{9}$$

Since L_{eq} is a function of L_1 to L_7, the minimization process gives the optimal values of such parameters. These parameters as discussed before are recognized as the deep saturation characteristic of the hysteretic inductors. A global solver, the simulated annealed algorithm is selected to solve the system of equations [30]. Note that, a gradient-based solver is avoided because these equations are highly nonlinear and thus the solution is sensitive to initial conditions.

$$L_{eq1}=\frac{2L_sA}{B}, \tag{7}$$
$$A=2L_6{}^2+2L_3L_4+L_3L_5+4L_3L_6+L_4L_5+2L_3L_7+2L_4L_6+L_5L_6+L_5L_7+2L_6L_7,$$
$$B=6L_6{}^2+6L_3L_4+3L_3L_5+12L_3L_6+3L_4L_5+6L_3L_7+6L_4L_6+3L_5L_6+3L_5L_7+6L_6L_7+18L_3L_s+2L_4L_s+4L_5L_s+10L_6L_s+2L_7L_s$$

This article has been accepted for publication in a future issue of this journal, but has not been fully edited. Content may change prior to final publication. Citation information: DOI 10.1109/TMAG.2016.2563389, IEEE Transactions on Magnetics

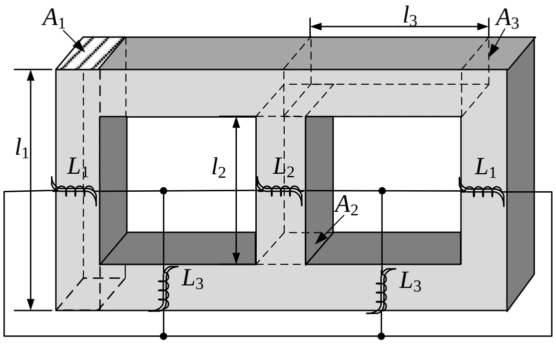

Fig. 4. Discretization of the iron core into sub-sections for the representation of the hysteretic inductors under the knee point.

C. Normal Open Circuit Condition

The high saturation part of the magnetizing branches (which is linear) mostly affect the magnitude and wave-shape of transients involving very deep saturation. In particular, for example, it affects the first peak of inrush currents. The nonlinear hysteretic part (below the knee point) is acquired to simulate the waveform of the inrush currents in low saturated condition (lower amplitude inrush currents). Also, the wave-shape and magnitude of the magnetizing current with nominal excitation is dependent on the accuracy of the hysteresis model below the knee point.

Efforts have been made to obtain all model parameters from terminal measurements. However, experience shows that accurate modeling of hysteresis under the knee point requires the magnetizing properties of the iron core as well as certain geometrical information of the core. The iron core is divided into several sections, comprising the three main sectional areas shown in Fig. 4; these are the middle leg, side legs, and yokes. Transformer manufacturers normally design the cross sectional area of legs and yokes in a way that ensures the flux density is uniform in all parts of the core when the transformer is excited under normal conditions. Therefore, it can be assumed that each part of the iron core is at the same degree of saturation, which means that the rectangular prisms (divisions) of the iron core as seen in Fig. 4 are physically sound. Note that, the shapes of the magnetizing currents, and consequently the shapes of the hysteresis loops obtained from simulations, are very sensitive to the proper selection of these subsections. Hence, the middle leg and the side legs sections are not selected with the same length. Comparison studies between simulations and experiments show that discretization pattern shown in Fig. 4 could lead to the most accurate representation of iron core electromagnetic behavior. Inductors L_1, L_2, and L_3 correspond to the side legs, middle leg, and yokes, respectively. Parameters l_1, l_2, and l_3 together with A_1, A_2, and A_3 are the corresponding lengths and cross sectional areas. Since the iron core is assumed to be uniformly excited, the *B-H* curve of the material can be transformed to a λ-i curve of the leg and the yoke components based on the iron core dimension as follows:

$$\lambda_p = NBA_p, \qquad i_p = \frac{Hl_p}{N}, \quad p = 1,2,3 \tag{10}$$

where B, H, N, λ, and i represent the flux density, magnetic field strength, number of turns, flux linkages, and current flowing in the coil, respectively. Note that, all inductors are referred to a common number of turns; N=1 in this paper. The turns-ratio of the windings are modeled with ideal transformers. The *B-H* curve of the iron core material is normally provided by the manufacturer for two flux densities (1.5 and 1.7 T) in the datasheets. In the case that the dimensions are not available, for example for the transformers that are already installed in the system, the estimation of the iron core dimensions with acceptable accuracy is possible; see [31].

D. Hysteresis Model

Hysteretic inductors (L_1, L_2, and L_3) in low- and high-saturated conditions (obtained in previous sections) need to be combined. In EMTP-type programs, hysteretic inductors are implemented by their offset characteristic λ-i curves. To insert their deep saturation behaviors, the unsaturated part of curves obtained by nominal tests (Section C), are extended at the last point with specific high saturation slopes, obtained from optimization routine (Section B), to infinity [22]. Additionally, linear air inductors are implemented in EMTP-RV [24].

Note that, the hysteretic components are rate dependent dynamic hysteresis models which consider the changes of hysteresis, eddy currents, and excess losses with respect to the voltage magnitude (excitation) and the frequency [26].

E. Short Circuit and Leakage Inductance

The transformer is short-circuited on the secondary (LV) and energized from the primary (HV) with a three-phase balanced source to measure the leakage inductance. The voltage is adjusted until the primary current reaches its nominal. The active power P_s, line voltage magnitudes U_{AB}, U_{BC}, U_{AC}, and phase current magnitudes $I_{A\varphi}$, $I_{B\varphi}$, $I_{C\varphi}$ are measured on the primary. The short-circuit voltage and current U_s and I_s, can be represented by [2]:

$$U_s = \frac{U_{AB} + U_{BC} + U_{AC}}{3}, I_s = \frac{I_{A\varphi} + I_{B\varphi} + I_{C\varphi}}{3} \tag{11}$$

The leakage inductance L_s can be calculated as:

$$L_s = \frac{1}{2\pi f k^2}\sqrt{\left(\frac{U_s}{\sqrt{3}I_s}\right)^2 - \left(\frac{P_s}{3I_s^{\,2}}\right)^2} \tag{12}$$

F. Winding Resistance

The resistance of the windings is measured with the method presented in [32]. The winding resistance is small and thus normal ohmmeter cannot offer enough accuracy. Hence, a Kelvin bridge is utilized to measure the winding resistances. Parameter R_w is the resistance of a phase winding. However, the measurements from the Δ and Y sides offer a combination of winding resistances in different phases. The measurement from the Y side is equivalent to the resistance of two winding in series (R_{wye}). The equivalent resistance measured from the Δ side is R_{delta} which is equivalent to the resistance of one of the windings in parallel with the other two in series. Hence,

$$R_w = \frac{R_{wye}}{2}; \quad R_w = \frac{3R_{delta}}{2} \tag{13}$$

Note that, the winding resistors need to be placed at the terminals of the corresponding ideal transformers.

III. CASE STUDY AND SIMULATION RESULTS

A three-phase transformer is modeled based on the principles described in previous sections. This transformer is 4.3 kVA, 120:120 V (ph-ph), 60 Hz, core-type, and without a tank. Each winding consists of 3 layers (68 turns per layer). Therefore, N=204 per winding. The detailed geometrical information can be found in the Appendix (see Fig. 9). The resistance of each winding is 0.4 ohm.

Because of the absence of a tank, hysteresis inductors that represent the tank (L_8 and L_9) are removed. Also, L_6 is replaced by linear air inductor. Since the circuit is symmetric, inductors L_3, L_4, and L_5 on the top part of the circuit and those on the bottom are merged. The simplified circuit is the same as the one presented in Fig. 2. The saturation inductances for the configuration shown in Fig. 3 are measured with the hybrid source method of [28]. As an alternative, finite element simulations are used to validate the measurements. The coils are energized with a dc voltage source in Comsol Multiphysics. The iron core is neglected since its permeability tends to unity in the very high saturation condition. Hence, it can be treated as air with μ=1. The i^{th} saturated inductor is calculated from the magnetic energy method:

$$L_{sati} = \frac{2\int \omega_m dv}{i_{i1}^{\,2}} \tag{14}$$

where ω_m is the magnetic energy density and i_1 is the dc source current. The comparison between simulations and measurements are provided in Table I. The differences are due to small measurement errors with available laboratory equipments and manufacturing deviations from the design specifications (errors in dimensions). The high saturation parts of the hysteretic inductors are then computed with (1) to (9). The leakage inductances are also computed with (11) and (12). The final numerical solutions and leakage inductance are given in Table II.

TABLE I
SATURATION INDUCTANCES SEEN FROM TERMINALS FOR ALL TEST CONFIGURATIONS COMPARED TO FEM SIMULATIONS

TEST	1	2	3	4	5	6	7
FEM (μH)	928	2886	3030	2255	2231	1442	1407
MEASUREMENTS (μH)	1047	2842	2820	2263	2342	1531	1481
DIFFERENCE (%)	11.4	1.6	7.5	0.4	4.7	5.8	5

TABLE II
PARAMETERS OF SATURATION INDUCTANCES OBTAINED FROM THE GLOBAL SOLVER

Inductance	L_1	L_2	L_3	L_4	L_5	L_6	L_7	L_s
μH	4160	5829	0	7138	15	2826	6672	1369

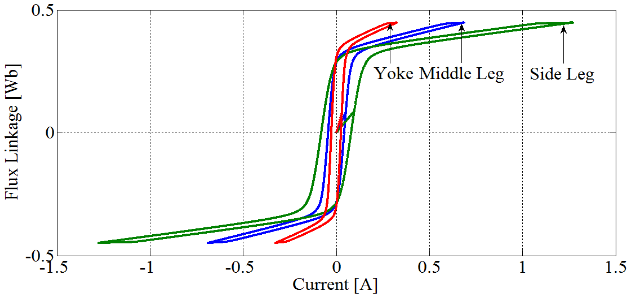

Fig. 5. λ-i curves of middle leg, side leg and yoke in the base of N=204 turns.

Note that, the solution for L_3 is zero. One can see from Fig. 1 that L_3 corresponds to the yokes. In high saturation, the iron core behaves very similar to air. Therefore, the three-leg transformer studied in this paper is magnetically equivalent to three independent coils in the air. As a result, a very low magnitude flux flows through the yokes. Hence, the obtained zero inductance (infinite reluctance) is physically sound for L_3 under deep saturation.

The λ-i curves calculated from the datasheet information and the dimensions of the core using (10) are illustrated in Fig. 5. This figure shows the difference between the characteristic of the hysteretic inductors (L_1, L_2, and L_3) below the knee point. The difference is due to the variation of the lengths and the cross sectional areas of the different parts of the core. One can see from the data in appendix that cross sectional areas of L_1, L_2, and L_3 are very close. Hence, the differences in flux axis are not visible.

The leakage inductances are also computed with (11) and (12). Finally, the model is implemented in EMTP-RV for validation.

A. Inrush Current

In this section, the model is validated comparing inrush current simulations and measurements. The transformer is excited with a three-phase balanced ac source. The device is demagnetized completely before each energization. The switch is closed at voltage zero-crossing moment of phase A. The same condition is simulated in the EMTP. The primary three-phase currents obtained from measurements and simulations are compared in Fig. 6. One can see that the model and simulations match in terms of the wave-shapes and the amplitudes.

The same test has been performed on the transformer from the secondary side, while the primary side is open circuit. The results are presented in Fig. 7. A very good agreement can be observed between the measurements and the simulation results. The relative differences of the peaks are 4.3%, 7.6%, and 1.5% for phases A, B, and C, respectively.

The results presented in this section show that the model is reversible and hence accurate to represent transients for both windings in the three phases.

B. Normal Open Circuit Condition

The transformer behavior under normal open circuit (nominal excitation) condition is evaluated in this section. Primary currents are recorded from measurements and compared with simulation results in Fig. 8.

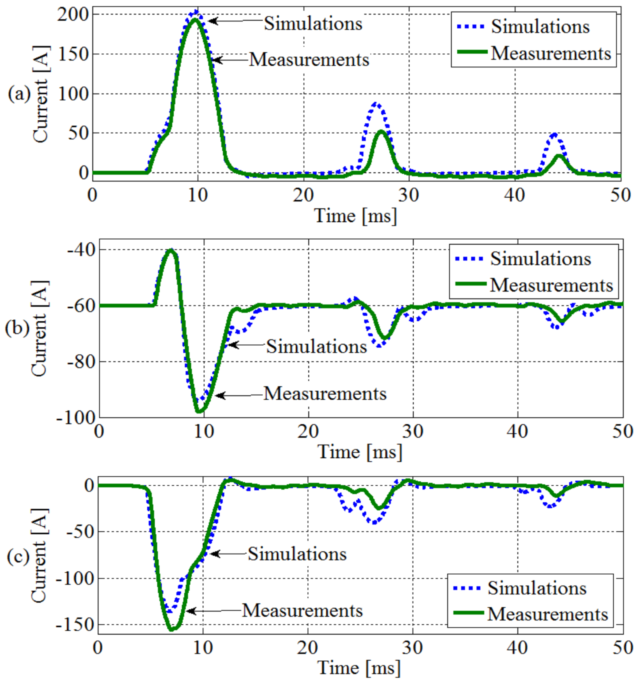

Fig. 6. Inrush current tests from primary side; (a) phase A, (b) phase B, (c) phase C.

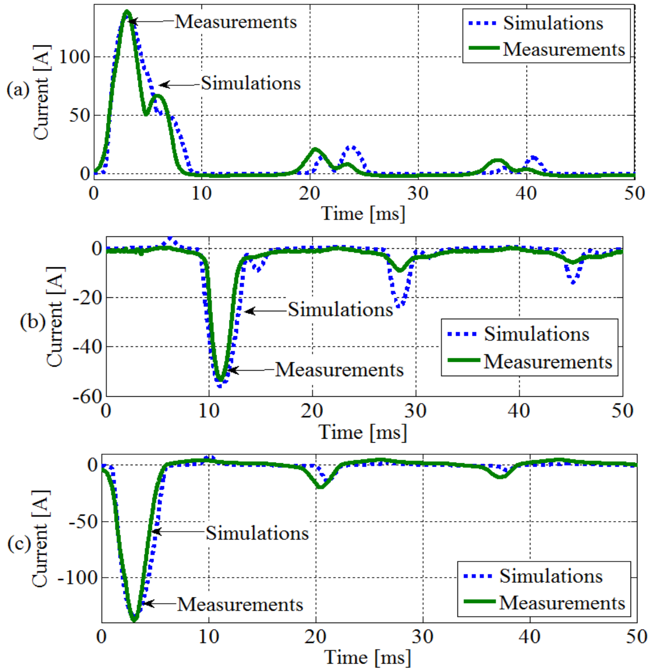

Fig. 7. Inrush current tests from secondary side: (a) phase A, (b) phase B, (c) phase C.

IV. CONCLUSION

In this paper, a dual reversible model has been developed for three-phase transformers. All components of the model correspond to a construction element of the transformer, since it is obtained from the application of the principle of duality. Step-by-step guidelines are provided to calculate the parameters and establish the model. It has been shown that only terminal measurements and physical size information are needed to build the model.

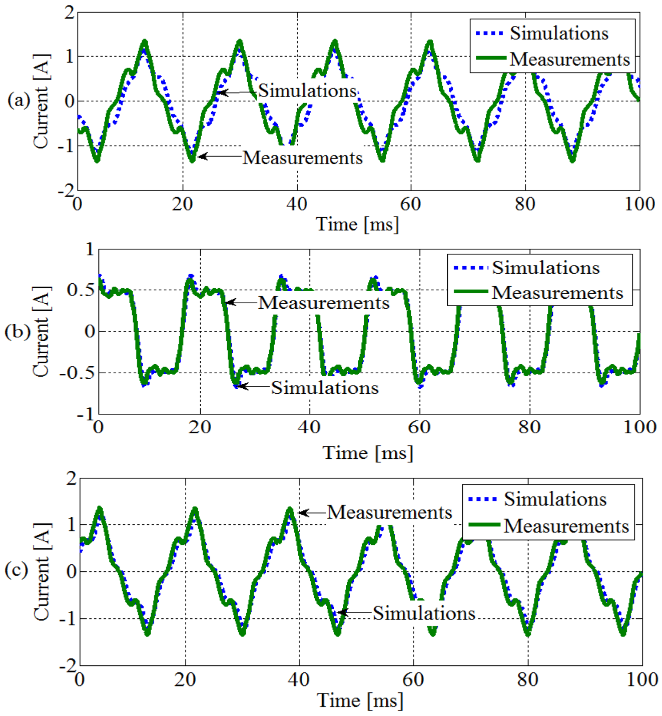

Fig. 8. Excitation current with nominal voltage in the open-circuit condition, (a) phase A, (b) phase B, (c) phase C.

The terminal response of the model is validated versus measurements from all windings. It has been demonstrated that the model is accurate for transients such as inrush currents seen for all the terminals without adjustment of the model parameters. The model also shows a very accurate response for the normal open circuit, loaded, and short circuit conditions.

APPENDIX

The geometrical information of the three-phase core-type transformer studied in this paper is given in Fig. 9.

REFERENCES

[1] J. A. Martínez and B. A. Mork, “Transformer modeling for low and mid-frequency transients—A review,” *IEEE Trans. Power Del.*, vol. 20, no. 2, pp. 1625–1632, Apr. 2005.

[2] J. A. Martínez, R. Walling, B. Mork, J. Martin-Arnedo, and D. Durbak, “Parameter determination for modeling systems transients. Part III: Transformers,” *IEEE Trans. Power Del.*, vol. 20, no. 3, pp. 2051–2062, Jul. 2005.

[3] Slow Transients Task Force of the IEEE, Modeling and Analysis of System Transients Using Digital Programs Working Group, “Modeling and analysis guidelines for slow transients—Part III: The study of ferroresonance,” *IEEE Trans. Power Del.*, vol. 15, no. 1, pp. 255–265, Jan. 2000.

[4] F. de León and A. Semlyen, “Complete transformer model for electromagnetic transients,” *IEEE Trans. Power Del.*, vol. 9, no. 1, pp. 231–239, Jan. 1994.

[5] A. Narang and R. H. Brierley, “Topology based magnetic model for steady-state and transient studies for three phase core type transformers,” *IEEE Trans. Power Sys.*, vol. 9, no. 3, pp. 1337–1349, Aug. 1994.

[6] B. A. Mork, F. Gonzalez, D. Ishchenko, D. L. Stuehm, and J. Mitra, “Hybrid transformer model for transient simulation—Part I: Development and parameters,” *IEEE Trans. Power Del.*, vol. 22, no. 1, pp. 248–255, Jan. 2007.

This article has been accepted for publication in a future issue of this journal, but has not been fully edited. Content may change prior to final publication. Citation information: DOI 10.1109/TMAG.2016.2563389, IEEE Transactions on Magnetics

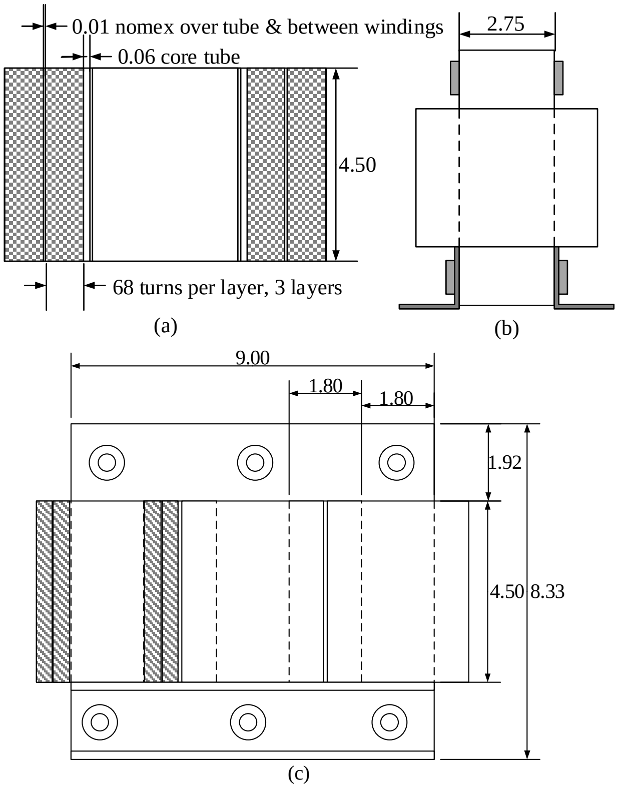

Fig. 9. Geometrical dimensions of the three-phase transformer under study. Note that the units are in inches.

[7] B. A. Mork, F. Gonzalez, D. Ishchenko, D. L. Stuehm, and J. Mitra, “Hybrid transformer model for transient simulation-part II: Laboratory measurements and benchmarking,” *IEEE Trans. Power Del.*, vol. 22, no. 1, pp. 256–262, Jan. 2007.

[8] A. Rezaei-Zare, “Enhanced transformer model for low-and mid-frequency transients—Part I: Model development,” *IEEE Trans. Power Del.*, vol. 30, no. 1, pp. 307–315, Feb. 2015.

[9] A. Rezaei-Zare, “Enhanced transformer model for low-and mid-frequency transients—Part II: Validation and Simulation Results,” *IEEE Trans. Power Del.*, vol. 30, no. 1, pp. 316–315, Feb. 2015.

[10] C. M. Arturi, “Transient simulation and analysis of a three-phase five-limb step-up transformer following and out-of-phase synchronization,” *IEEE Trans. Power Del.*, vol. 6, no. 1, pp. 196–207, Jan. 1991.

[11] X. Chen and S. S. Venkata, “A three-phase three-winding core-type transformer model for low frequency transient studies,” *IEEE Trans. Power Del.*, vol. 12, no. 2, pp. 775–782, Apr. 1997.

[12] F. de León and J. A. Martínez, “Dual three-winding transformer equivalent circuit matching leakage measurements,” *IEEE Trans. Power Del.*, vol. 24, no. 1, pp. 160–168, Jan. 2009.

[13] N. Chiesa, B. A. Mork, and H. K. Høidalen, “Transformer model for inrush current calculations: Simulations, measurements and sensitivity analysis,” *IEEE Trans. Power Del.*, vol. 25, no. 4, pp. 2599–2608, Oct. 2010.

[14] R. Yacamini and H. Bronzeado, “Transformer inrush calculations using a coupled electromagnetic model,” in *Proc. Inst. Elect. Eng., Sci. Meas. Technol.*, vol. 141, pp. 491–498, Nov. 1994.

[15] X. Wang, D. W. P. Thomas, M. Sumner, and J. Paul, “Characteristics of Jiles-Atherton model parameters and their application to transformer inrush current,” *IEEE Trans. Magn.*, vol. 44, no.3, pp.340-345, Mar. 2008.

[16] E. Cardelli, E. Della Torre, V. Esposito, and A. Faba, “Theoretical considerations of magnetic hysteresis and transformer inrush current,” *IEEE Trans. Magn.*, vol. 45, no.11, pp.5247-5250, Nov. 2009.

[17] E. Cardelli, A. Faba, and F. Tissi, “Prediction and control of transformer inrush currents,” *IEEE Trans. Magn.*, vol. 51, no.3, pp.1-4, Mar. 2015.

[18] J. Faiz and S. Saffari, “Inrush current modeling in a single-phase transformer,” *IEEE Trans. Magn.*, vol. 46, no.2, pp.578-581, Feb. 2010.

[19] B. A. Mork, “Five-legged wound-core transformer model: Derivation, parameters, implementation, and evaluation,” *IEEE Trans. Power Del.*, vol. 14, no.4, pp. 1519-1526, Oct. 1999.

[20] T. Tran-Quoc and L. Pierrat, “An efficient nonlinear transformer model and its application to ferroresonance study,” *IEEE Trans. Magn.*, vol. 31, no.3, pp. 2060-2063, May. 1995.

[21] S. E. Zirka, Y. I. Moroz, C. M. Arturi, N. Chiesa, and H. K. Høidalen, “Topology-correct reversible transformer model,” *IEEE Trans. Power Del.*, vol. 27, no. 4, pp. 2037–2045, Oct. 2012.

[22] S. Jazebi, F. de León, A. Farazmand, and D. Deswal, “Dual reversible transformer model for the calculation of low-frequency transients,” *IEEE Trans. Power Del.*, vol. 28, no. 4, pp. 2509–2516, Oct. 2013.

[23] S. Jazebi and F. de León, “Experimentally validated reversible singe-phase mutli-winding transformer model for the accurate calculation of low-frequency transients,” *IEEE Trans. Power Del.*, vol. 30, no. 1, pp.193–201, Feb. 2015.

[24] *“DCG-EMTP (Development coordination group of EMTP) Version EMTP-RV, Electromagnetic Transients Program,”* [Online]. Available: http://www.emtp.com

[25] S. Jazebi, S. E. Zirka, M. Lambert, A. Rezaei-Zare, N. Chiesa, Y. Moroz, X. Chen, M. Martinez-Duro, C. M. Arturi, E. P. Dick, A. Narang, R. A. Walling, J. Mahseredjian, J. A. Martinez, and F. de León, “Duality Derived Transformer Models for Low-Frequency Electromagnetic Transients –Part I: Topological Models,” IEEE *Trans. Power Del.*, Early Access.

[26] S. E. Zirka, Y. I. Moroz, N. Chiesa, R. G. Harrison, and H. Kr. Hoidalen, “Implementation of inverse hysteresis model into EMTP – Part II: dynamic model,” *IEEE Trans. Power Del.*, Early Access.

[27] S. E. Zirka, Y. I. Moroz, and C. M. Arturi, “Accounting for the influence of the tank walls in the zero-sequence topological model of a three-phase, three-limb transformer,” *IEEE Trans. Power Del.*, vol. 29, no. 5, pp. 2172–2179, Oct. 2014.

[28] F. de León, S. Jazebi, and A. Farazmand, “Accurate measurement of the air-core inductance of iron-core transformers with a non-ideal low-power rectifier,” *IEEE Trans. Power Del.*, vol. 29, no. 1, pp. 294–296, Feb. 2014.

[29] Q. Wu, S. Jazebi, and F. de León, “System of equations for parameter estimation of three-phase reversible dual transformer models for low-frequency transient studies from terminal measurements,” *NYU internal report*. September 2015. Available upon request from the authors.

[30] S. Kirkpatrick, C. D. Gelatt, and M. P. Vecchi, “Optimization by Simulated Annealing,” *Science*, *New Series*, vol. 220, no. 4598, pp. 671-680, May 1983.

[31] S. Mitchell and J. Welsh, “Initial parameter estimates and constraints to support gray box modelling of power transformers,” *IEEE Trans. Power Del.*, vol. 28, no. 4, pp. 2411–2418, Oct. 2013.

[32] *IEEE Standard Test Code for Liquid-Immersed Distribution, Power, and Regulating Transformers*, IEEE Standard C57.12.00, 2010.

[33] G. Shirkoohi, “Dependence of magnetization near saturation on alloying content in ferromagnetic steel,” *IEEE Trans. Magn.*, vol. 51, no. 7, pp. 1-10, Jun. 2015.

[34] D. K. Rao and V. Kuptsov, “Effective use of magnetization data in the design of electric machines with overfluxed regions,” *IEEE Trans. Magn.* , vol. 51, no. 7, pp. 1-9, Jul. 2015.

[35] T. D. Kefalas and A. G. Kladas, “Analysis of transformers working under heavily saturated conditions in grid-connected renewable energy systems,” *IEEE Trans. Ind. Electron.*, vol. 59, no. 5, pp. 2342-2350, May 2012.